

# On the Application of Dynamic Fracture Mechanics to Continuous Fiber Reinforced Composite Materials

J.J. Mason

Department of Aerospace and Mechanical Engineering  
University of Notre Dame  
Notre Dame, Indiana 46556

19970602 088

## 1 Introduction

While many investigations have been directed toward understanding quasi-static crack growth in fiber reinforced composite materials, surprisingly little effort has been applied to understanding dynamic crack growth in these materials. Certainly, this effort should be made since composites are increasingly being used in applications where they may be exposed to impact, dynamic loading or energetic failure i.e. in airplane skin, submarine walls, pressure vessels and automobiles. Under such circumstances dynamic crack growth is a probable failure mechanism.

There are many dynamic failure mechanisms in fiber reinforced composite materials; the five major mechanisms are splitting, delamination, transverse fracture, fiber pull-out and debonding.[1] Splitting involves crack propagation along the fiber direction. Delamination involves crack propagation between laminates or layers. Transverse fracture indicates crack growth perpendicular to the fiber direction. Fiber pull-out relates to the cracking of fibers and their subsequent sliding in the matrix. And, debonding indicates a loss of bond between fiber and matrix without fiber cracking. Under dynamic loading the composite material actually fails by a complex competition between each of these mechanisms. Naturally, the failure mechanism of the composite depends upon the properties of the constituents, the matrix and fiber, and the bond between them. These properties, in turn, determine the

DISTRIBUTION STATEMENT A  
Approved for public release;  
Distribution Unlimited

strength of each mechanism and whether that mechanism acts during dynamic composite failure. The nature of dynamic crack growth, the propagation of a single dominant flaw—and whether or not it occurs at all, is determined by all of these factors; the material properties and the strength associated with each possible mechanisms of failure.

The impact resistance of composites materials *has* been well investigated and several interesting conclusions can be drawn.[1] The energy absorbing ability of the composite is directly related to the energy absorbing ability of the fiber. The Mode II (shear crack) properties of the matrix tend to determine the amount of damage in the composite. The strength of the bond between matrix and fiber may be decreased to increase energy absorption but at the cost of permanent damage to the material. The fiber stacking sequence plays a significant role in determining the failure mode. The geometry of the test may have effects on the results. Scalability is not to be assumed. And, *there is a distinct dependency of the failure mode selection upon the rate of loading*. However, impact resistance of composites is generally tested under conditions of either low or high velocity impact on thin plates perpendicular to the plate surface[1][2] where the predominant modes of failure are delamination and damage, respectively. A single dominant flaw is not often observed.

If loading is in the plane of the plate rather than perpendicular to it—as is the case in internally pressurized cylinders, explosion within cylinders, edge impact of plates, end impact of cylinders, dynamic bending of large structures and many other cases—dynamic propagation of a single flaw, or a localized damage zone that is equivalent to a single flaw, may be the mode of failure. This, of course, depends upon the rate of loading, the nature of the composite lay-up and the constituent properties just like in impact problems.

In the work reported here the goals are to examine crack initiation and propagation in plates of unidirectional fiber reinforced composites where the loading is limited to act within the plane of the plate. To that end, an experimental and analytical approach was described in the grant proposal. In brief, that method indicated examination, both visually and interferometrically using ultra-high speed photography, of the failure of unidirectional

composite materials loaded in-plane. At this point in the study two materials have been identified; one is a fiber reinforced epoxy material used in the manufacture of composites mirrors and the other is a model material, glass fiber reinforced polycarbonate or polymethyl methacrylate, that is being produced at Notre Dame. The first material is a high fiber density material that was chosen because it can be readily acquired in a reflective state suitable for interferometry. The latter material is used to demonstrate the effects of low fiber density on crack initiation and propagation and to contrast or verify the findings of studies on the higher density fiber materials. Furthermore, the low density material may be used to explore dynamic crack interactions with a single fiber

Two experimental thrusts were initially identified, the one point bend or three point bend tests which lead to mode I crack propagation were to be used as was the Kalthoff test which leads to mode II crack propagation. At this point, findings from other studies have demonstrated that the Kalthoff and the one point bend tests have severe limitations in the duration of dynamic loading of the notch tip.[3] Consequently, in the interest of increasing load duration, the three point bend test will be used and a variation on the Kalthoff test called the Two Dimensional Dynamic Punch Test has been developed here at Notre Dame. The analysis presented in the following section indicates the advantages of a dynamic punch test. Namely, the conditions under which a Two Dimensional Dynamic Punch Test produces a larger stress intensity factor than the Kalthoff tests are outlined.

## 2 Theoretical Analysis of Dynamic Punch Test

Two tests and two materials have been identified in this study, the dynamic punch test and the dynamic three point bend test as well as the high density unidirectional fiber reinforced epoxy and the low density unidirectional model material. In this section<sup>1</sup> stress intensity factors for side impacted isotropic plates and edge notched specimens are examined. The specimens are initially at rest and the projectile is rigid. Impact of the rigid projectile is

---

<sup>1</sup>The contents of this section was co-authored by K.M. Roessig and has been submitted for publication in *Engineering Fracture Mechanics*.

modeled by a constant velocity condition on the impact surface. Three support geometries are considered for each specimen geometry: a free back surface, a fixed back surface, and a two dimensional punch. Analytical approximations for the stress intensity factor history are given for short times, while dynamic quarter point finite element solutions are included for longer times. The stress intensity factor is shown to increase with time due to wave reflection in the two dimensional punch and fixed back support geometries, while it decreases with time for the free back surface. The stress intensity factors in the plate specimen are also greater than those in the edge notched specimen in all tests. For applicability to manufacturing operations and increased chance of shear dominated failure, it is recommended that the two dimensional punch or fixed back surface geometries of the plate specimen be used in experimental studies.

## 2.1 Introduction

The purpose of this paper is to examine the stress intensity factor histories of impact experiments used to study shear dominated failure in metals, polymers, and composites.

In metals, this type of shear dominated fracture is commonly preceded by adiabatic shear localization. Adiabatic shear localization is a material instability in which thermal softening overcomes strain and strain rate hardening in a material [4]. This localization usually occurs at higher loading rates, and can collapse into very thin bands. Failure by this mechanism can lead to lower failure energies. Adiabatic shear bands occur in many applications including ballistic impact, explosives, metal forming, and manufacturing operations such as punching and blanking. In punching operations, adiabatic shear localizations can form at the corner of the punch, but also at the back of the specimen at the corner of the die. See Figure 1 where a contour plot of plastic equivalent strain in an axisymmetric punching simulation of a titanium alloy is shown. Two shear localizations are present, one at the corner of the punch and one at the corner of the die. The formation and interaction of these localizations can have a dramatic effect on the energy and displacement to failure of the material [5].

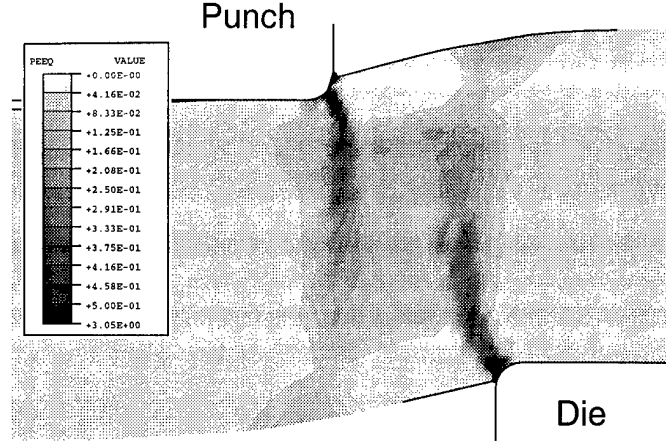


Figure 1: Contour plot of plastic equivalent strain in an axisymmetric punching simulation. Two shear localizations are present, one at the corner of the punch and one at the corner of the die. (Roessig and Mason, 1997)

In polymers and polymer based composites, shear dominated failure is also observed [6]. In impact studies of edge notched polycarbonate specimens, a transition from a tensile dominated brittle fracture mode to a shear dominated ductile fracture mode is observed with increasing impact velocities. The brittle fracture mode is dominated by crazing, similar to fracture observed in polymethyl methacrylate (PMMA) [7], and grows in the direction of maximum tensile normal stress. The ductile fracture mode propagates in the direction of maximum shear stress, and extensive ductile deformation is evident on the fracture surface. The ductile fracture arrests during the test, suggesting that energy absorption is much higher for this fracture mode.

Current tests to examine shear failure include the torsional split Hopkinson bar (TSHB) [8, 9, 10], an axisymmetric punch test [5], and side impact of edge notched specimens [11, 12, 13]. Both high strain rates and deformation on exterior surfaces are desirable experimentally. High strain rates lead to a greater chance of shear dominated failure, and deformation on the exterior surfaces makes experimental techniques such as high speed photography and temperature measurements possible. For these reasons, the impact of edge notched specimens has become popular (see Figure 2d), but this test produces complete shear failure only for a select group of materials. Also, the applicability of the geometry to manufacturing

applications is currently limited.

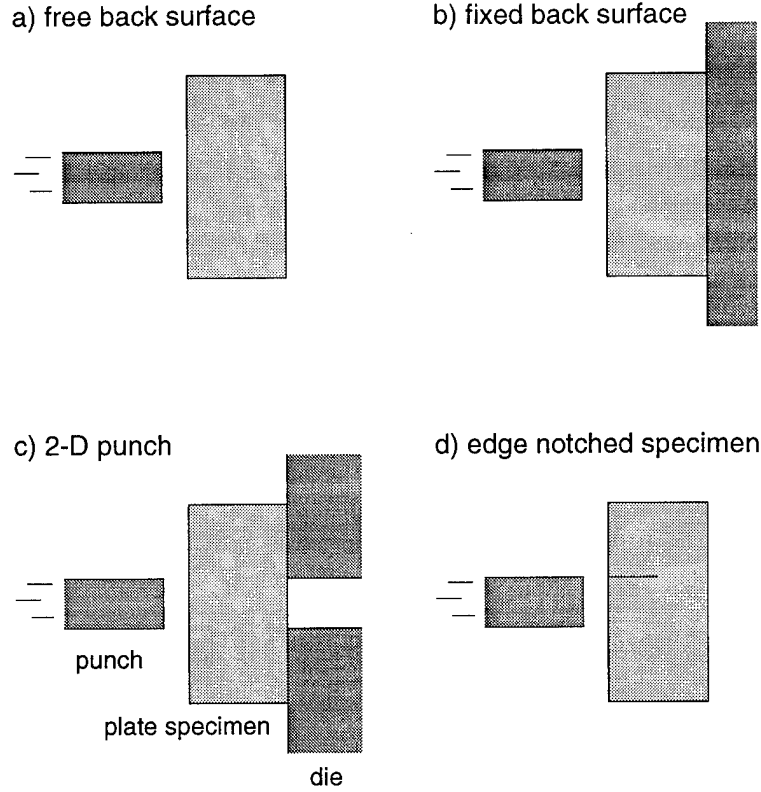


Figure 2: Plate specimen in the a) free surface, b) fixed surface, and c) two dimensional punch geometries. The edge notched specimen d) is also used in each geometry.

However, the initiation of adiabatic shear bands in metals is generally determined by a critical strain criterion [4] and shear failure of polymers may be determined by a similar criterion. Assuming small scale yielding until initiation, Chen and Batra have proposed that this critical strain criterion is equivalent to a critical stress intensity factor criterion [14]. For this reason, the stress intensity factor histories of the punch test and side impact edge notched plate test should be examined. Lee and Freund [15] have already calculated the mode I and mode II stress intensity factor histories for the impact of an edge notched specimen, but there appears to be no calculation of the stress intensity factor history in a dynamic punch test. An examination of the long time stress intensity factor histories of the side impacted edge notched plate and of a two dimensional punch test will reveal the applicability and usefulness of the side impacted edge notched plate tests to manufacturing

and ballistic impact problems. Furthermore, analysis of the stress intensity factor history in dynamic punch tests may allow the use of this test in place of a side impacted edge notched plate test making it possible to test a larger range of materials in shear dominated failure modes.

Two different specimen geometries are examined. The plate specimen is a solid rectangular piece of material, 50mm×100mm in size. The edge notched specimen has the same dimensions, but a notch of length 25mm has been introduced 35mm from the top as shown schematically in Figure 2. Impact occurs centered in the middle of the side face. The punch width is set to 30mm, placing the projectile impact just below the notch in the edge notched specimens. For each specimen, three support geometries are used. The free back surface places no constraint on the specimen, while the fixed back surface restricts displacement in the direction of the projectile impact of the edge opposite the impacted edge. The two dimensional punch geometry fixes the displacement in the direction of projectile impact for the area in contact with the die only. The rest of the material is under no constraints. The clearance between the projectile and die is 1mm; that is, the gap in the die shown in Figure 2c is 2mm larger than the punch width. A two dimensional punch geometry is used as an approximation to the axisymmetric punch test. A two dimensional representation of the axisymmetric punch test is valid as long as the stresses and displacements are only examined close to the corner of the punch or die, when the distance to the punch or die is much smaller than the punch or die radius. The definition of the stress intensity factor includes the limit as the radius approaches zero, so this condition is satisfied and a plane strain solution approximates the axisymmetric solution [16]. Figure 2 shows the two specimen types and the three support geometries. Elastic, plane strain conditions are assumed throughout the analysis and all material parameters, where applicable, are for steel ( $E=200\text{GPa}$ ,  $\nu=0.3$ ,  $\rho=7840\text{ kg/m}^3$ ).

## 2.2 Calculation of Dynamic Stress Intensity Factor for a Two Dimensional Punch Test

The stress intensity factor history for the impact of a two dimensional elastic half space by a rigid punch can be determined by using an equivalent geometry. A rigid punch impact can be replaced by a compressive plane wave impinging two semi-infinite cracks, see Figure 3. The particle motion due to the plane wave is in a downward vertical direction, and as the wave reaches the cracks, the displacement history becomes the superposition of an internally pressurized crack and an uncracked solid. An equivalent displacement history of the impinging wave is a downward velocity condition of the line between the two cracks, which, by neglecting the upper crack face, is the representation of a rigid punch impact. Therefore, the rigid punch impact can be modeled by a compressive plane wave impinging two semi-infinite cracks. The analysis to follow neglects any contact of the crack faces, which will not occur in a two dimensional punch test, and thus allows for interpenetration of the crack faces.

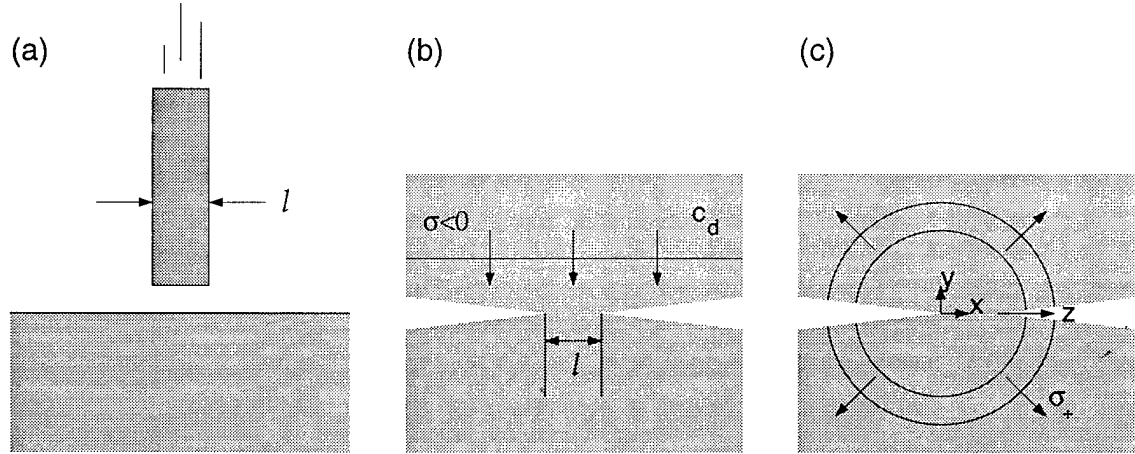


Figure 3: The stress intensity factor of a rigid punch impacting an elastic half space (a) can be determined by examining a plane compression wave impinging on two semi-infinite cracks (b). Reflected waves will be generated (c) which will cause the stress state to change in the opposite crack.

Freund [17] states that the stress intensity factor history of a plane wave impinging a semi-infinite crack can be described by a semi-infinite crack loaded internally by a suddenly

applied pressure. Similar to the displacement field, the complete stress field differs only by the additional stress of the pulse propagating through an uncracked solid. But as this stress pulse does not generate singular stresses, the stress intensity factor can be calculated from the internal pressure loading only. This has been done by Freund [17] with the use of the Weiner-Hopf technique and shown to be proportional to the square root of time. The exact relation is

$$K^{(0)}(t) = 2\sigma^* \frac{\sqrt{c_d t (1 - 2\nu) / \pi}}{(1 - \nu)}, \quad (1)$$

where  $c_d$  is the plane strain dilatational wave speed,  $\nu$  is the Poisson's ratio for the material, and  $\sigma^*$  is the magnitude of the stress pulse. This solution will be altered at later times by crack tip interactions, hence the notation  $K^{(0)}(t)$  is used.

As the plane wave encounters the cracks, the pulse will be partially scattered by the crack tips. The normal stresses generated by the scattered waves from one crack tip will at some later time reach the other semi-infinite crack, see Figure 3c. At that time, Equation (1) is no longer valid. Stresses equal and opposite to those scattered by the first crack must be generated along the second crack to keep the crack faces stress free, thereby changing the stress intensity factor at the second crack tip. The change in the stress intensity factor,  $K^{(1)}(t)$ , must be added to the semi-infinite crack solution,  $K^{(0)}(t)$ , to obtain the total stress intensity factor history,

$$K(t) = K^{(0)}(t) + K^{(1)}(t) \quad (2)$$

Due to symmetry, a similar change is seen at the first crack tip. The stress distribution from the scattered wave along the  $x$  axis in front of the crack tip,  $\sigma_+$ , has also been calculated by Freund and is given by the equation

$$\sigma_+(x, t) = -\frac{1}{\pi x} \int_{ax}^t \text{Im} \left\{ \Sigma_+ \left( -\frac{\eta}{x} \right) \right\} d\eta \ H(t - ax), \quad (3)$$

where  $H$  is the Heaviside function,  $t$  is time,  $a$  is the inverse of the dilatational wave speed,  $c_d$ , and  $\Sigma_+$  is the Laplace transform of  $\sigma_+$ , the details of which are given by Freund [17]. A plot of this normalized stress distribution is given in Figure 4.

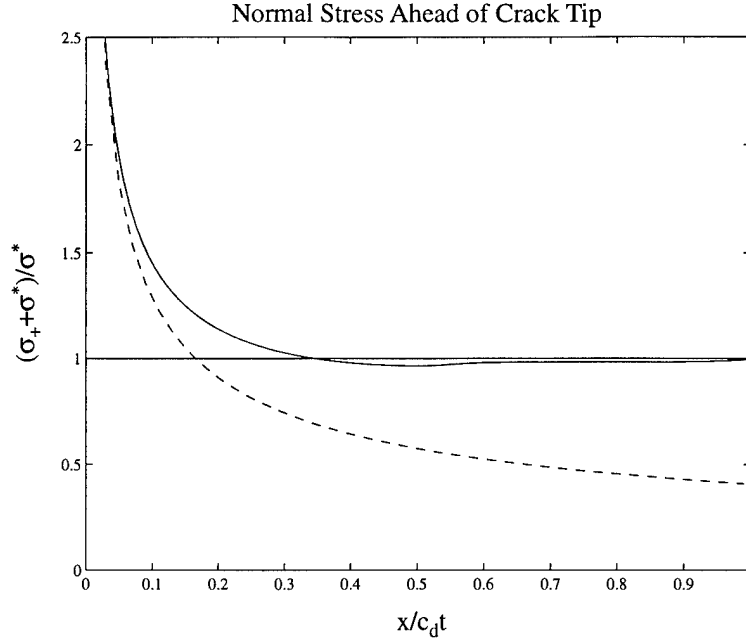


Figure 4: Normal stress ahead of the crack tip versus normalized distance  $x/c_d t$  for plane compression pulse of magnitude  $\sigma^*$  impinging on a semi-infinite crack. The solid curve is the complete stress distribution and the dashed curve is the singular field only. (Freund, 1990)

At any given time, the stress distribution from Equation (3) is known. The stress intensity factor from the scattered stress wave must now be determined and added to the stress intensity factor from Equation (1). Freund calculates the stress intensity factor at a crack tip for a point load at a distance  $l_p$  from the crack tip. This stress intensity factor can be integrated as a Green's function to determine the stress intensity factor history at the crack tip for a temporally and spatially varying stress distribution. The distribution in question is the one shown in Figure 4. The time history of the stress intensity factor at the crack tip for a point load,  $K_p$ , is shown in Figure 5. The normalization factor is the equilibrium value  $K_p(\infty) = p^* \sqrt{2/\pi l_p}$  where  $p^*$  is the magnitude of the applied load.

The integral of the stress intensity distribution begins with the equation

$$K^z(t, z) = \int_{0^-}^t K_p(t-s, z) \dot{\sigma}_+(s, z) ds, \quad (4)$$

where  $z = x - l$ . The final Green's integral becomes

$$K^{(1)}(t) = \int_0^{c_d t - l} K^z(t, z) dz \quad (5)$$

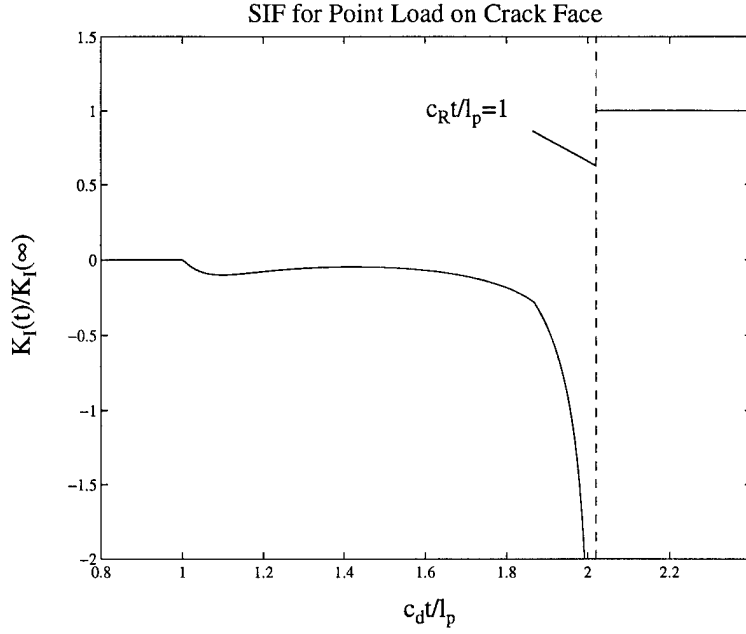


Figure 5: Normalized stress intensity factor for a point load at a distance  $l_p$  from the crack tip. The normalization factor is the equilibrium value,  $K_p(\infty)$ . (Freund, 1990)

$$= \int_0^{c_dt-l} \int_{0^-}^t K_p \left( \frac{c_d(t-s)}{z} \right) \dot{\sigma}_+ \left( \frac{z+l}{c_d s} \right) ds dz \quad (6)$$

where  $l$  is the punch width as shown in Figure 3. The equations are non-dimensionalized by the following transformations:

$$t^* = \frac{c_dt}{l}, \quad (7)$$

$$s^* = \frac{c_d s}{l}, \quad (8)$$

$$\xi = \frac{z}{l}. \quad (9)$$

Substitution of the non-dimensional variables and switching the order of integration leads to

$$K^{(1)}(t^*) = \frac{l^2}{c_d} \int_0^{t^*} \int_0^{t^*-1} K_p \left( \frac{t^* - s^*}{\xi} \right) \dot{\sigma}_+ \left( \frac{\xi + 1}{s^*} \right) d\xi ds^*. \quad (10)$$

The two terms in the integrand must be examined more closely. The data for the  $K_p$  term is in non-dimensional form, so during the integration, it must be dimensional. Therefore, the first multiplicative term in the integrand is multiplied by  $\sigma^* \sqrt{2/(\pi l_p)}$ . The variable  $l_p$  represents the distance of the point load to the crack tip, which in terms of the variables in

the integral equation corresponds to  $z$ . Once non-dimensionalized, the final multiplicative correction is

$$\sigma^* \sqrt{\frac{2}{\pi l}} \frac{1}{\sqrt{\xi}}, \quad (11)$$

where  $\sigma^*$  is the magnitude of the stress pulse, equal to  $\rho c_d V_p$  from elastodynamics, and  $V_p$  is the magnitude of the velocity condition imposed on the elastic body.

The time derivative of the stress distribution must be changed into a derivative with respect to the non-dimensional variable it is plotted against. The chain rule is invoked to obtain

$$\dot{\sigma} = \frac{d\sigma}{dt} = \frac{\partial \sigma_+}{\partial \left( \frac{\xi+1}{s^*} \right)} \left( -\frac{\xi+1}{s^{*2}} \right) \left( \frac{c_d}{l} \right) \quad (12)$$

Substitution of the above relation into the integral leads to the following equation,

$$K^{(1)}(t^*) = -\sigma^* \sqrt{\frac{2l}{\pi}} \int_0^{t^*} \int_0^{t^*-1} K_p \left( \frac{t^* - s^*}{\xi} \right) \dot{\sigma}_+ \left( \frac{\xi+1}{s^*} \right) \left( \frac{\xi+1}{s^{*2} \sqrt{\xi}} \right) d\xi ds^*. \quad (13)$$

The above equation can be simplified in a number of ways. For time integration, the interval of  $0 < s^* < 1$  can be neglected since the wave diffracted from one crack tip has not yet reached the other. The integrand is therefore zero in this interval, and the limits on  $s^*$  can be changed from  $[0, t^*]$  to  $[1, t^*]$ . The limits on  $\xi$  can also be changed by examining the  $\dot{\sigma}$  term. For  $\xi \geq s^* - 1$ , the term is equal to zero. This is due to the fact that one only needs to integrate up to the distance that the stress distribution has reached for the given time. Therefore the limits on  $\xi$  can be changed to  $[0, s^* - 1]$ . Finally, another transformation can be used to remove the square root singularity in  $\xi$ . By making the transformation

$$\eta = \sqrt{\xi}, \quad (14)$$

the integral equation becomes

$$K^{(1)}(t^*) = -2\sigma^* \sqrt{\frac{2l}{\pi}} \int_1^{t^*} \int_0^{\sqrt{s^*-1}} K_p \left( \frac{t^* - s^*}{\eta^2} \right) \dot{\sigma}_+ \left( \frac{\eta^2 + 1}{s^*} \right) \left( \frac{\eta^2 + 1}{s^{*2}} \right) d\eta ds^*. \quad (15)$$

By recognizing the fact that the stresses must be of opposite sign to keep the crack faces stress free, the negative sign can be dropped. Also dividing by  $K_o = \sigma^* \sqrt{2l/\pi}$  gives a

non-dimensional form for  $K(t^*)$ . The final equation for the change in stress intensity factor history at the corner of the punch is

$$\frac{K^{(1)}(t^*)}{K_o} = 2 \int_1^{t^*} \int_0^{\sqrt{s^*-1}} K_p \left( \frac{t^* - s^*}{\eta^2} \right) \dot{\sigma} \left( \frac{\eta^2 + 1}{s^*} \right) \left( \frac{\eta^2 + 1}{s^{*2}} \right) d\eta ds^*. \quad (16)$$

Discontinuities in the integrand, as shown in Figure 5 for example, warranted the evaluation of this integral using the trapezoidal rule. This solution is only valid from  $l/c_d < t < 2l/c_d$ , from the time the scattered wave first reaches the opposite crack tip until the time that the scattered wave returns to the crack tip from which it was generated.

For the two dimensional punch geometry, another stress singularity occurs where the specimen meets the corner of the die. The stress wave that propagates across the specimen will meet this surface and cause further wave reflection and diffraction. For the plate specimen, this situation can be thought of as a plane compressive wave impinging on a finite length interior crack, see Figure 6. By the same reasoning as for the two semi-infinite cracks, the stress intensity factor for an interior crack loaded by a compressive plane wave is the same as an internally pressurized finite length crack. The only difference in stress state is that of a compressive plane wave moving through an *uncracked* solid, which does not affect the stress intensity factor. The wave traveling through the plate specimen will not be a plane wave, exactly, but it will be approximated as such. In the edge notch specimen, this line of reasoning will not be valid as the wave impinging on the die surfaces will not be closely approximated by a plane wave.

The solution to the problem of an internally pressurized crack is also given by Freund [17], and is another integral equation. If  $K_f^{(0)}(t)$  is the stress intensity factor for the semi-infinite crack, in this case the variation of  $K_f^{(0)}(t)$  at each time,  $K_f^{(1)}(t)$ , is given, as

$$K_f^{(1)}(t) = -\frac{2\sigma^* F_+(0)}{\pi} \sqrt{\frac{2l_f}{\pi}} \int_a^{\eta^*} \text{Im} \left\{ \frac{\sqrt{\eta^* - \eta} F_-(\eta)}{\eta F_+(\eta)} \right\} d\eta \quad (17)$$

where  $l_f$  is the finite crack length and  $\eta^* = t/l_f$ . The function  $F$  is complex and is described in detail by Freund. This equation is valid from  $l_f/c_d < t < 2l_f/c_d$ , when the first reflected wave reaches the opposite crack tip to when the first reflected wave returns to its original

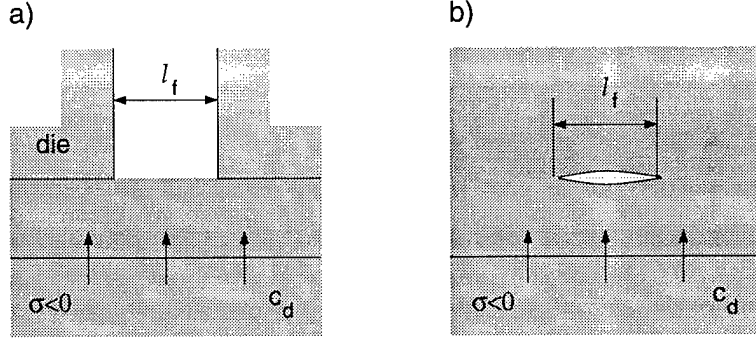


Figure 6: A plane wave in the specimen impinging on a die can be represented by a plane wave impinging a finite length crack in the interior of an elastic body.

crack tip. The total normalized stress intensity factor for the interior crack is given by

$$K_f(t) = K_f^{(0)}(t) + K_f^{(1)}(t) \quad (18)$$

and is plotted in Figure 7. The normalization factor is the equilibrium value of  $K_f(\infty) = \sigma^* \sqrt{\pi l_f/2}$ .

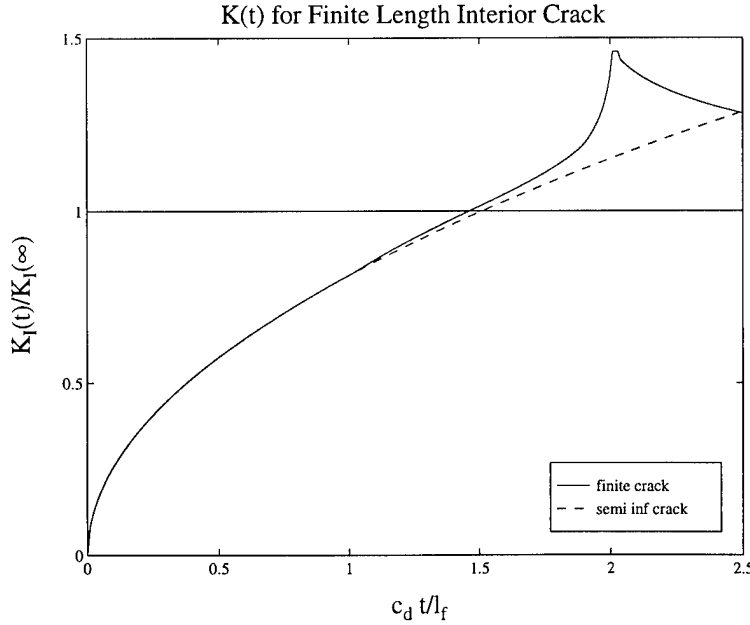


Figure 7: Transient stress intensity factor versus normalized time for an interior crack loaded by a plane compressive wave. The dashed line is the result for the semi-infinite crack. The stress intensity factor is normalized by the equilibrium value,  $K_f(\infty)$ . After  $c_d t/l_f = 2.5$ , the stress intensity factor decays to its normalized equilibrium value of 1. (Freund, 1990)

## 2.3 Finite Element Modeling

The finite element package ABAQUS/Standard was used to examine the long time behavior of the specimens after impact. Both the plate and edge notched specimens were examined, as shown in Figure 2. Collapsed 8-node, plain strain, quarter point elements (QPE) were used to model the singularity at the corners of the punch in the plate and around the notch tip in the edge notched specimens.

The different boundary conditions of the various geometries were modeled by constraining the appropriate nodes. For the fixed surface, all the nodes on the back surface were constrained in the direction of the punch velocity, while for the free surface no nodes were constrained. For the two dimensional punch geometry, the nodes that represent the die in Figure 2 were constrained. At the corners of the die, QPE were again used to model the stress singularity. The punch was approximated by placing a velocity condition on the relevant nodes. Symmetry was used in the plate specimen to reduce computational effort.

Attention must be given to the time step used for dynamic crack analysis. The time increment,  $\Delta t$ , must be less than the characteristic time,  $\tau_c$ , defined as

$$\tau_c = \frac{h}{c_d} \quad (19)$$

where  $h$  is the element size [18]. This ensures a high degree of accuracy by preventing the fastest traveling wave from moving across an entire element in one time increment. A minimum time step also occurs, and is labeled the critical time increment,  $\Delta t_{cr}$ . This minimum is a fraction of the characteristic time,

$$\Delta t_{cr} = \eta \tau_c \quad (20)$$

where  $\eta$  depends on the integration scheme being used [18]. For the Newmark- $\beta$  method.

$$\eta = \frac{0.1}{\beta} \quad (21)$$

For time steps below this critical value, spurious oscillations are present and can become

unbounded. Therefore the appropriate time increment has a range given by the relation

$$\frac{0.1}{\beta} \tau_c \leq \Delta t \leq \tau_c. \quad (22)$$

Stress intensity factors were calculated from the finite element displacement data from the quarter point elements. For the edge notch specimen, the mode I and II stress intensity factors can be calculated according to Murti and Valliappan [18] by the relations

$$K_I(t) = \sqrt{\frac{2\pi}{l_c}} \frac{G}{4(1-\nu)} [4(u'_a(t) - u'_d(t)) - (u'_b(t) - u'_c(t))] \quad (23)$$

$$K_{II}(t) = \sqrt{\frac{2\pi}{l_c}} \frac{G}{4(1-\nu)} [4(v'_a(t) - v'_d(t)) - (v'_b(t) - v'_c(t))]. \quad (24)$$

where  $l_c$  is length of the QPE, and  $u$  and  $v$  are displacements defined in Figure 8. These equations are obtained by equating the first two terms of the Williams series expansion [19] and the finite element displacements in the vicinity of the crack.

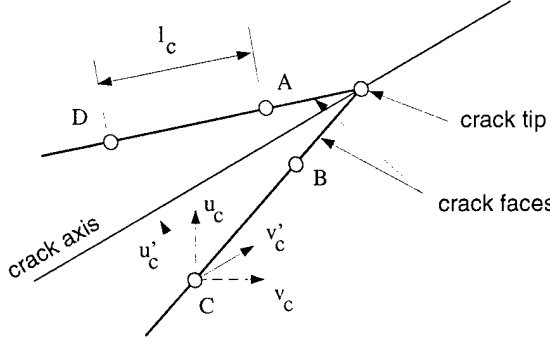


Figure 8: Displacement definitions for calculation of notch tip stress intensity factors. (Murti and Valliappan, 1986)

For the plate specimen, there is only one surface, so another method must be used. By using an Airy stress function approach, Nadai [20] found the stresses and displacements in an elastic half space indented by a rigid punch. The boundary conditions restrict all stresses to be zero along the free surface while the shear stress is also zero along the surface under the punch. The normal stress is square root singular under the punch. With the corner of the punch at the origin, with  $\theta=0$  corresponding to the free surface and  $\theta = \pi$  corresponding

to the surface under the punch, the solution for the stresses is

$$\sigma_{rr} = -\frac{3}{4} \frac{c}{\sqrt{r}} \left( \sin\left(\frac{3\theta}{2}\right) + 5 \sin\left(\frac{\theta}{2}\right) \right) \quad (25)$$

$$\sigma_{\theta\theta} = -\frac{3}{4} \frac{c}{\sqrt{r}} \left( -\sin\left(\frac{3\theta}{2}\right) + 3 \sin\left(\frac{\theta}{2}\right) \right) \quad (26)$$

$$\tau_{r\theta} = -\frac{3}{4} \frac{c}{\sqrt{r}} \left( \cos\left(\frac{3\theta}{2}\right) - \cos\left(\frac{\theta}{2}\right) \right) \quad (27)$$

where  $c$  is a constant.

A stress intensity factor in terms of the constant  $c$  can now be determined by the following definition,

$$K = \lim_{r \rightarrow 0} \sqrt{2\pi r} \sigma_{\theta\theta} (\theta = \pi). \quad (28)$$

Solving for  $c$  yields

$$c = -\frac{K}{3\sqrt{2\pi}}. \quad (29)$$

The displacement equations are now given as

$$u_r = \frac{K}{4G} \sqrt{\frac{r}{2\pi}} \left[ \sin\left(\frac{3\theta}{2}\right) + (5 + 8\nu) \sin\left(\frac{\theta}{2}\right) \right], \quad (30)$$

$$u_\theta = \frac{K}{4G} \sqrt{\frac{r}{2\pi}} \left[ \cos\left(\frac{3\theta}{2}\right) + (7 - 8\nu) \cos\left(\frac{\theta}{2}\right) \right]. \quad (31)$$

The stress intensity factor can be determined in terms of one displacement,  $u_\theta$ , at the free surface. Substituting  $\theta = 0$  and rearranging leads to the final expression for  $K$ ,

$$K(t) = \frac{G}{(1 - \nu)} \sqrt{\frac{\pi}{2r}} u_\theta(r, t). \quad (32)$$

## 2.4 Results

Figure 9 shows the results of the integration for the stress intensity factor at the corner of a rigid punch on a semi-infinite plate. The solid line is the stress intensity factor for a single semi-infinite punch, given by Equation (1). The dashed line represents the stress intensity factor including the first diffracted wave from the opposite punch corner. The reflected wave first has an effect at  $c_d t/l=1$ , which corresponds to the arrival of the wave. This solution is

exact only until  $c_d t/l=2$ , which corresponds to the arrival of the reflection from the opposite corner of the pulse initially generated at the first corner. The correction,  $K^{(1)}(t)$ , has minimal effect initially because the magnitude of the scattered stress pulse is initially very small, see Figure 4. Because the stress remains small for some time, the calculation neglecting multiple reflections of scattered waves serves as a good approximation of the stress intensity factor beyond  $c_d t/l=2$ . In this regime, the stress intensity factor initially increases slightly over that of the single semi-infinite punch, and then decreases as the stress wave,  $\sigma_+(x, t)$ , changes sign at later times. The difference, though, is very small; at a non-dimensional time of 10 it is only about 12%. The finite element data is shown by the circles falling between the two solutions. In the finite element calculation, infinite elements were used on the back and side boundaries so that no wave reflections would occur from these surfaces. In the finite specimens shown in Figure 2, the arrival of the first wave reflected from the back surface occurs at a non-dimensional time of 3.33. Up to this time, the three different curves agree very well. Therefore, up to the first wave reflection, the stress intensity factor equation for the single semi-infinite punch, Equation (1), can be used with excellent accuracy for  $\sigma^* = \rho c_d V_p$ .

The stress intensity factors at the corner of the punch for the fixed and free surface geometries for the plate specimen are shown in Figure 10. The stress intensity factor for the free back surface drops as the reflected wave is tensile and the contact surface between the punch and die is unloaded. The reflected wave from the fixed back surface has an opposite effect as the this pulse is compressive, and increases the load on the punch. The interesting feature is that the increase or decrease in the stress intensity factor can be approximated by the addition of another semi-infinite punch stress intensity factor history from Equation (1). For the free back surface, unloading case, the solid line represents the unloading that would be experienced if the pulse reflected from the back surface was a semi-infinite tensile pulse of magnitude  $\sigma^* = \rho c_d V_p$  or the input velocity condition was a finite length pulse. Further additions of unloading waves are not needed as the projectile will lose contact with the

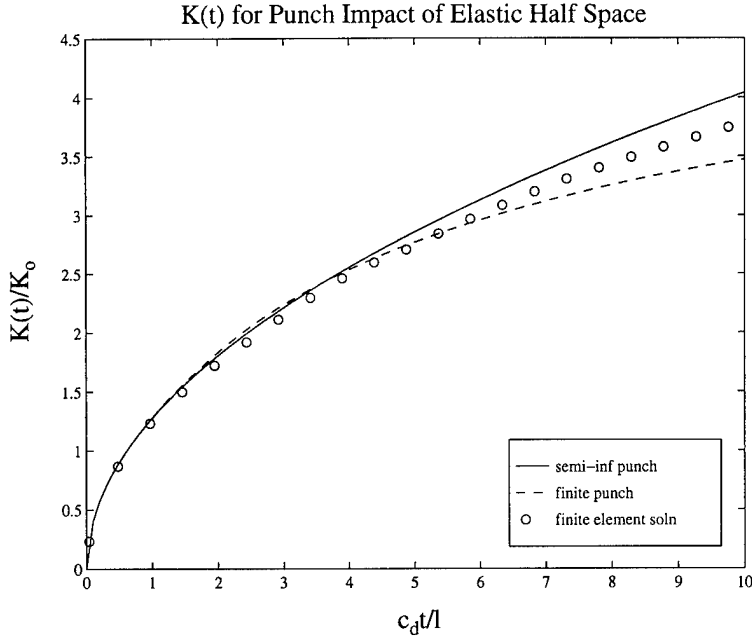


Figure 9: Normalized stress intensity factor against normalized time for impact of elastic half-space.

specimen after the first reflection. For the fixed back surface, a reflected wave is expected at the punch corner every  $t^*=3.33$ , and adding semi-infinite compressive wave loadings of magnitude  $\sigma^* = \rho c_d V_p$  at appropriate times predicts the stress intensity factor very well out to  $t^*=10$  as shown by the solid lines. Further additions of compressive loading stress intensity factors may lead to accurate approximations for  $K$  at longer times. Wave reflections from the top and bottomed surfaces are present and cause some error, but surprisingly, prediction is still good.

For the edge notched specimen, the finite element short time behavior, shown in Figure 11a, agrees very well with the solution of Lee and Freund [15] which is valid until the  $c_dt/l=2.5$  using the normalization  $K_o = \sigma^* \sqrt{2l/\pi}$ , which is the time at which the reflected pulses from the back and impact surfaces return to the notch tip. Figure 11 shows that at the end of Lee and Freund's solution,  $c_dt/l=2.5$ , the stress intensity factor for the fixed and free surface geometries diverge as the reflected waves are of different sign. The stress intensity factor histories are different than the histories for the plate specimen in Figure 10

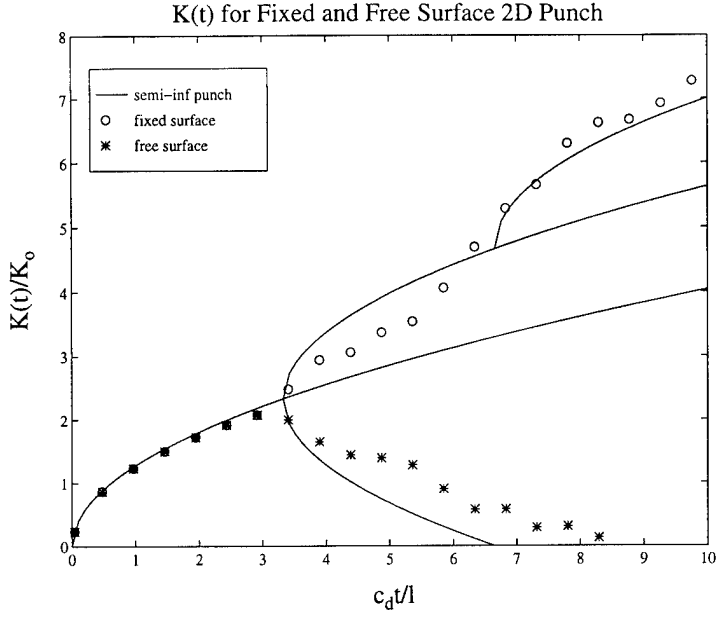


Figure 10: Normalized stress intensity factor against normalized time for the two dimensional punch geometry with fixed and free back surfaces.

due to the nature of the specimen geometry. For long times, Figure 11b, the trends are the same when  $K$  for the punch test is compared to  $K_{II}$  for the edge notched specimen. The stress intensity factor decreases for the specimens with a free back surface and increases for the fixed back surface geometry. Comparisons are not made between the stress intensity factor for the punch geometry and  $K_I$  in the edge notched specimens because the focus of this work is on shear dominated failure.

The final geometry, the two dimensional punch geometry, is different from the previous geometries in that part of the back surface is fixed, and part is free. In this case, there will also be a stress singularity at the corner of the die on the back surface. Figure 12 shows the stress intensity factor histories for the plate and edge notched specimens under identical impact velocities in the two dimensional punch geometry with the stress intensity factor at the die included. The stress intensity factor for the edge notched specimen is plotted for  $c_dt/l - l_n/l$  so that comparisons can be made between the magnitude of the stress intensity factor in the punch test and edge notched specimen. For the plate specimen, there is an initial drop in the stress intensity factor at the punch corner as the initial part of the returning wave is tensile,

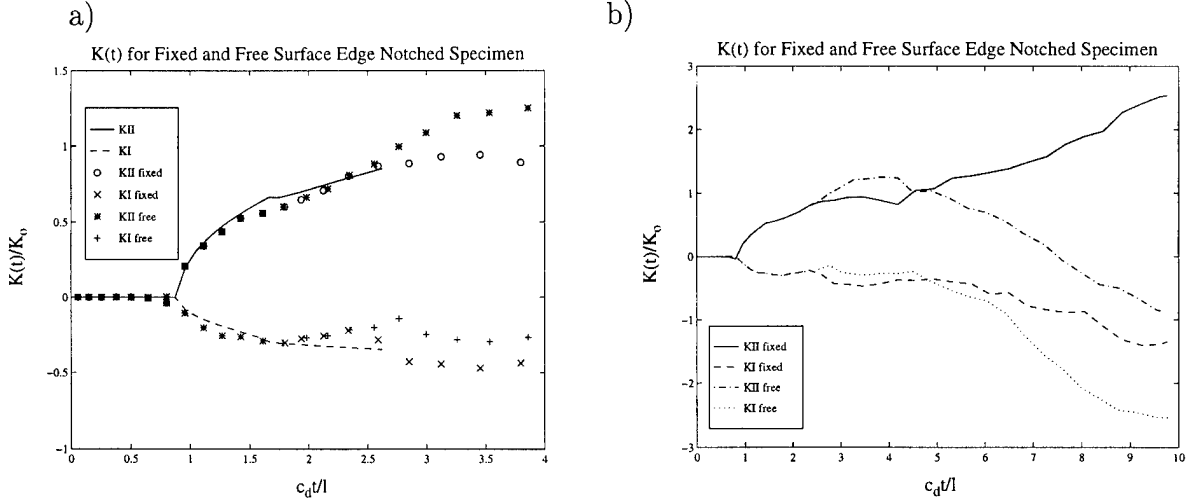


Figure 11: Normalized stress intensity factor against normalized time for the edge notched specimen with fixed and free back surfaces. Plot a) is for short times and compares well with the analytical solution by Lee and Freund (1990), while plot b) shows the stress intensity factor at longer times.

but it eventually rises. The same type of behavior is seen for the edge notched specimen, though it is not as pronounced. The most notable aspect is that the stress intensity factor for the plate specimen is higher than the edge notched specimen for all times. The prediction of the stress intensity factor at the die corner of the plate specimen from the interior crack approximation is quite good for small times after the arrival of the wave. The analytical stress intensity factor agrees until an approximate time of  $t^*=4$ , at which time the analytical expression begins to decay to its equilibrium value. This is because the analytical expression is for a single incident pulse with no reflections, which is not the case in the finite element analysis. The semi-infinite punch stress intensity factor continues to increase in time beyond  $t^*=4$  but underestimates the finite element stress intensity factor by as much as 40%. The stress intensity factor for the die corner for the edge notched specimen does not agree with the interior crack approximation as the incident wave is not a plane wave, nor can it be closely approximated by one.

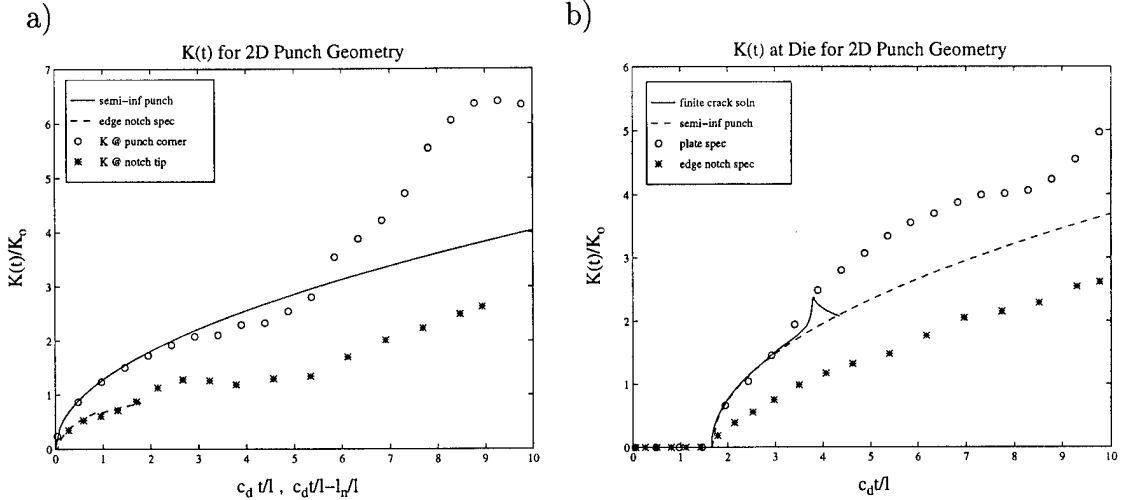


Figure 12: Normalized stress intensity factor against normalized time for the plate and edge notch specimens in the two dimensional punch geometry. Plot a) shows the stress intensity factor at the punch corner and notch tip and plot b) shows the stress intensity factor at the die corner.

## 2.5 Conclusions

The study of shear dominated failure is very important to many fields, including ballistics and manufacturing. In punching applications, shear dominated failure may occur in multiple locations and stress intensity factors may possibly be used to characterize and predict that failure. Knowing the stress intensity factor histories during the impact event aids in the prediction of the initiation of shear failure. Also with the solution in hand, a two dimensional punch test can be performed which allows for greater understanding of shear dominated failure in axisymmetric cases.

In this work, it has been shown that before any wave reflections occur, the simple expression for the stress intensity factor of a single semi-infinite crack, Equation (1), is a very good approximation for the plane wave loading of two semi-infinite cracks, which is equivalent to the rigid punch problem. Successive additions or subtractions, for fixed or free back faces respectively, of the single crack stress intensity factor history can be performed for each wave reflection in the plate specimen until  $c_d t/l=10$ , and possibly beyond, but only when the back face is either fixed or free. In the two dimensional punch test approximate closed

form solutions are valid only until  $c_d t/l=5$ .

Analysis of two specimen geometries in three support configurations reveals much information about the loading during punch tests. Between the two specimen types, the trends are the same for each support configuration. The stress intensity factor decreases for the free back surface configuration upon the arrival of the tensile reflected wave; the stress intensity factor increases upon the arrival of the reflected wave for the fixed back surface configuration. Since the fixed surface has a completely compressive reflected wave, the stress intensity factor increases more quickly than in the punch configuration. Overall, however, the plate specimens were found to have higher stress intensity factors than the edge notched specimens at the same impact velocity. The two dimensional punch and fixed back surface support geometries allowed for a monotonically increasing stress intensity factor in time, while the free back surface caused unloading of the specimens and a decrease in stress intensity factor.

Future tests which study shear dominated failure in metals, polymers, or composites, should use the plate specimen in a two dimensional punch or fixed back surface support geometry to allow for a greater stress intensity factor and higher probability of shear dominated failure.

### 3 Experimental Investigations

While theoretical analyses were being performed on the Two Dimensional Dynamic Punch Test to demonstrate its advantages over other mode II dominated tests such as the Kalthoff test, preparations were being made for experimental investigations of both mode I and mode II crack propagation in composite materials.

First, it was necessary to develop the ability to manufacture model composite materials with low fiber density. These materials are to be examined in conjunction with the high fiber density composites in an effort to illuminate the effects of crack bridging and crack/fiber interactions through comparisons and contrasts. For this purpose, a mold was designed and built to manufacture the composites. The mold uses two sheets of matrix material

to sandwich the fibers. Clamps are added to apply pressure to the polymer sheets. It was necessary to include heating elements to raise the temperature of the polymer matrix material above its glassy transition temperature making it easier to form the composite, and it was also necessary to lap and polish the mold components optically flat to produce specimens that would be usable in interferometric study. Capabilities for the production of such composites were not previously available at Notre Dame, and difficulties with machining the mold caused delays in the preparation of this mold. Several attempts were made to form composites using several materials systems in the mold. Eventually, the use of E-glass fibers in either a polycarbonate or polymethyl methacrylate matrix were identified as moldable systems. Polycarbonate shows particular promise as a model material because of its demonstrated shear failure capability.[6] Model composites are currently being successfully made.

Also, an order was placed to Composite Mirror Applications, Inc. for high density fiber composites. Twelve suitable specimens were ordered in September of 1996. They were completed and delivered in April of 1997

Last, the ability to dynamically load specimens at Notre Dame was improved. Basically, this entailed the manufacture of a specimen holding devise that will allow testing in the Two Dimensional Dynamic Punch Test and the three point bend test to be performed with ease and repeatability. The specimen holder is mounted on the end of an air gun barrel as shown in Figure 13(a). The punch tests will be performed using a die with inserts shown in Figure 13(b). Provisions have been made for performing three point bend tests using the die and inserts.

Tests of the composites will begin in June, 1997.

## 4 Second Year of Work

Presently, all the factors are in place to begin the core of the work outlined in the research proposal for this grant. The work over the next year will be focussed on achieving the following goals:

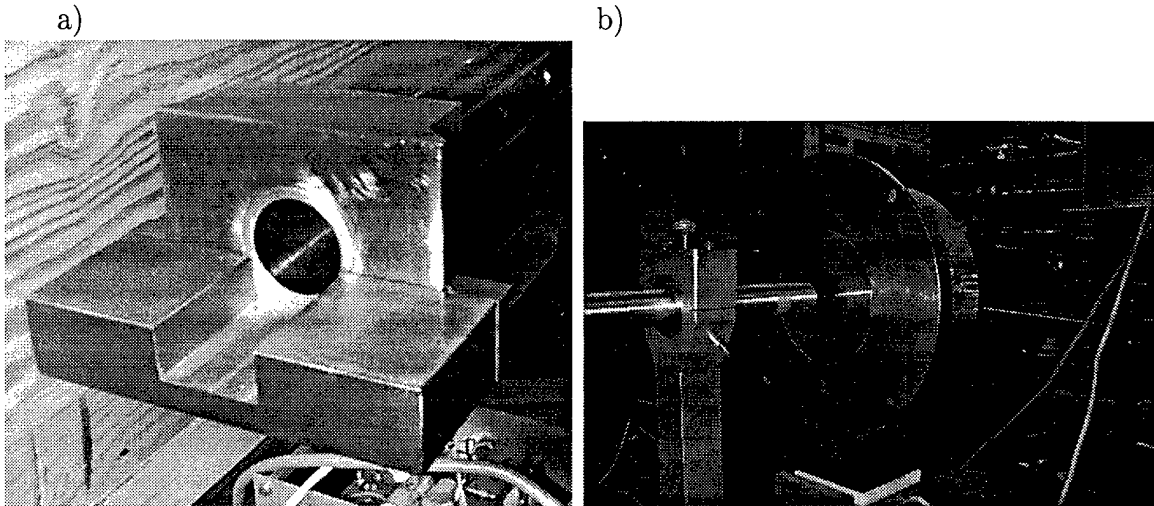


Figure 13: Loading devices prepared; (a)specimen holding device and (b) die support.

- (I) Tests of each of the composite materials, high density epoxy matrix, low density polycarbonate matrix and low density polymethyl methacrylate, under dynamic mode I and mode II loading will be performed. Post mortem examination of the failure mode will be made as will high speed, white light observation of the failure event. Comparisons will be made between different failure modes as well as between different loading schemes. Expected completion date for these experiments, September 1997.
- (II) Quasistatic interferometry of the materials will be performed in mode I dominated loading. Expected completion date, September 1997
- (III) Ultra-high speed interferometry of the tests listed in (I) will be performed to record quantitative information about the deformation history leading to initiation of failure and the failure process itself. Attention will be paid to the effects and nature of crack/fiber interactions. Expected completion date of experiments, January 1998.
- (IV) An experimental technique using a shearing interferometer that reduces the laser light intensity by 25% rather than by 75%, like CGS,[21] will be developed.

Expected completion date, May 1998.

- (V) Three dimensional numerical analysis of punch test on anisotropic materials will be performed with attention paid to the order of singularity and the validity of a plane stress assumption in the experiments mentioned in (I)-(III). Expected completion date, January 1998.
- (VI) Modeling of the experiments in (I), (II) and (III) will begin in January 1998 with emphasis on using crack tip zones to characterize the observed initiation and propagation of cracks. Expected completion date, May 1998.

The third year will be dedicated to investigations of more complicated materials such as multiple layered materials and materials with woven reinforcement fibers.

## 5 Summary

The first year of work has entailed mostly preparations for experiments which have included the design, manufacture and verification of a composite manufacturing system, acquisition of premanufactured composite mirrors and manufacture of a specimen loading system. Analysis of the tests has also begun with an analysis of shear dominated loading systems as described in section 2 of this report. The results of the analysis indicate that back support of the Kalthoff and dynamic punch test leads to higher stress intensity factors and a longer duration of loading in the singular zone. Interestingly, the Two Dimensional Dynamic Punch Test has a larger stress intensity factor than the Kalthoff test as described in the analysis.

Work in the next year will focus on experiments and numerical models of those experiments. Experiments will be performed quasistatically and dynamically with emphasis on observation of the initiation and propagation of failure and the acquisition of qualitative and quantitative descriptions of that failure. Models will initially examine the shear and tensile dominated loading of cracks and plates with emphasis on anisotropic materials under

plane stress conditions. Later models will focus on the implementation of bridging in crack initiation and propagation as observed in the various experiments.

## References

- [1] W.J. Cantwell and J. Morton. The impact resistance of composite materials—a review. *Composites*, 22(5), 1991.
- [2] S. Abrate. Impact on laminated composite materials. *Applied Mechanics Reviews*, 44(4), 1991.
- [3] J.J. Mason, J.A. Zimmerman, and K.M. Roessig. The effect of aging condition on shear localization at the tip of a notch in maraging steels. *submitted to J. Mat. Sci.*, 1997.
- [4] Y. Bai and B. Dodd. *Adiabatic Shear Localization: Occurrence, Theories and Applications*. Pergamon Press, New York, 1992.
- [5] K.M. Roessig and J.J. Mason. Adiabatic shear localization in the axisymmetric punch test. *submitted to Int. J. of Plasticity*, 1997.
- [6] K. Ravi-Chandar. On the failure mode transitions in polycarbonate under dynamic mixed mode loading. *Int. J. Solids Structures*, 32(6/7):925–938, 1995.
- [7] P.D. Washabaugh and W.G. Knauss. Nonsteady periodic behavior in dynamic fracture of pmma. *Int. J. Fracture*, 59:187–197, 1993.
- [8] A. Marchand and J. Duffy. An experimental study of the formation process of adiabatic shear bands in a structural material. *J. Mech. Phys. Solids*, 36(3):251–283, 1988.
- [9] J.H. Giovanola. Adiabatic shear banding under pure shear loading, Part I: Direct observation of strain localization and energy dissipation measurements. *Mechanics of Materials*, 7:59–71, 1988.

- [10] J.H. Giovanola. Adiabatic shear banding under pure shear loading, Part II: Fractographic and metallographic observations. *Mechanics of Materials*, 7:73–87, 1988.
- [11] J.F. Kalthoff and S. Wrinkler. Failure mode transition at high rates of shear loading. In C.Y. Chiem, H.-D. Kunze, and L.W. Meyer, editors, *Impact Loading and Dynamic Behavior of Materials*, pages 185–195, 1987. Vol. 1.
- [12] J.J. Mason, A.J. Rosakis, and G. Ravichandran. Full field measurements of the dynamic deformation field around a growing adiabatic shear band at the tip of a dynamically loaded crack or notch. *J. Mech. Phys. Solids*, 42(11):1679–1697, 1994.
- [13] M. Zhou, A.J. Rosakis, and G. Ravichandran. Dynamically propagating shear bands in impact-loaded prenotched plates I. Experimental investigations of temperature signatures and propagation speed. *J. Mech. Phys. Solids*, 44(6):981–1006, 1996.
- [14] L. Chen and R.C. Batra. Analysis of thermoviscoelastic instability at an impact loaded crack tip. *unpublished*, 1997.
- [15] Y.J. Lee and L.B. Freund. The stress intensity factor due to normal impact loading of the faces of a crack. *Int. J. Engng Sci.*, 12:179–189, 1974.
- [16] R. Hill. *The Mathematical Theory of Plasticity*. Oxford University Press, London, England, 1964.
- [17] L.B. Freund. *Dynamic Fracture Mechanics*. Cambridge University Press, Cambridge, NY, 1990.
- [18] V. Murti and S. Valliappan. The use of quarter point elements in dynamic crack analysis. *Engineering Fracture Mechanics*, 23(3):585–614, 1986.
- [19] M.L. Williams. On the stress distribution at the base of a stationary crack. *Journal of Applied Mechanics*, 24:109–114, March 1957.

- [20] A. Nadai. *Theory of Flow and Fracture of Solids*, volume 2. McGraw-Hill Book Company, 1963.
- [21] A.J. Rosakis. Two optical techniques sensitive to gradients of optical path difference: the method of caustics and the coherent gradient sensor. In J.S. Epstein, editor, *Experimental Techniques in Fracture*, page 327. VCH Pub., New York, 1993.

# REPORT DOCUMENTATION PAGE

Form Approved  
OMB No. 0704-0188

Public reporting burden for this collection of information is estimated to average 1 hour per response, including the time for reviewing instructions, searching existing data sources, gathering and maintaining the data needed, and completing and reviewing the collection of information. Send comments regarding this burden estimate or any other aspect of this collection of information, including suggestions for reducing this burden to Washington Headquarters Services, Directorate for Information Operations and Reports, 1215 Jefferson Davis Highway, Suite 1204, Arlington, VA 22202-4302, and to the Office of Management and Budget, Paperwork Reduction Project (0704-0188), Washington, DC 20503.

1. AGENCY USE ONLY (Leave blank)		2. REPORT DATE 27 May 97	3. REPORT TYPE AND DATES COVERED Annual, 1 June 96 - 31 May 97
4. TITLE AND SUBTITLE  On the Application of Dynamic Fracture Mechanics to Continuous Fiber Reinforced Composite Materials		5. FUNDING NUMBERS  G ND0014-96-0774 PR 96PR05511-00	
6. AUTHOR(S)  J. J. Mason		8. PERFORMING ORGANIZATION REPORT NUMBER	
7. PERFORMING ORGANIZATION NAMES(S) AND ADDRESS(ES)  University of Notre Dame Department of Aerospace & Mechanical Engineering 365 Fitzpatrick Hall Notre Dame, IN 46556		9. SPONSORING / MONITORING AGENCY NAMES(S) AND ADDRESS(ES)  Office of Naval Research 800 N. Quincy St. Arlington, VA 22217-5660	
11. SUPPLEMENTARY NOTES  Portions of this report have been submitted for publication in <i>Engineering Fracture Mechanics</i> .		10. SPONSORING / MONITORING AGENCY REPORT NUMBER	
a. DISTRIBUTION / AVAILABILITY STATEMENT  Approved for public release; distribution unlimited.		12. DISTRIBUTION CODE	
13. ABSTRACT (Maximum 200 words)  Progress is reviewed with emphasis on a model of stress intensity factors in dynamic punch test. The specimen is assumed to be initially at rest and the projectile is rigid. Impact of the rigid projectile is modeled by a constant velocity condition on the impact surface. Three support geometries are considered for each specimen geometry: a free back surface, a fixed back surface, and a two dimensional punch. Analytical approximations for the stress intensity factor history are given for short times, while dynamic quarter point finite element solutions are included for longer times. The stress intensity factor is shown to increase with time due to wave reflection in the two dimensional punch and fixed back support geometries, while it decreases with time for the free back surface. The stress intensity factors in the plate specimen are also greater than those in the edge notched specimen in all tests. For applicability to manufacturing operations and increased chance of shear dominated failure, it is recommended that the two dimensional punch or fixed back surface geometries of the plate specimen be used in experimental studies.			
14. SUBJECT TERMS  Stress intensity factor, dynamic fracture, punch test, quarter point elements		15. NUMBER OF PAGES 29	16. PRICE CODE
17. SECURITY CLASSIFICATION OF REPORT Unclassified	18. SECURITY CLASSIFICATION OF THIS PAGE Unclassified	19. SECURITY CLASSIFICATION OF ABSTRACT Unclassified	20. LIMITATION OF ABSTRACT UL